

Coupling of orthogonally polarized waves in LiNbO₃ optical waveguides

D. Kip, R. Fink, T. Bartholomäus and E. Krätzig

Universität Osnabrück, Barbarastraße 7, W-4500 Osnabrück, Germany

Received 13 May 1992; revised manuscript received 15 September 1992

In LiNbO₃ waveguides light is converted from ordinary to extraordinary polarization. We use a simple model to describe this effect, especially the dependence on the geometric properties (thickness, cut direction) of the waveguides. We report results for linear and circular photovoltaic tensor elements of iron- and copper-doped lithium niobate waveguides.

1. Introduction

Besides materials like GaAs, doped glasses or polymers, LiNbO₃ is of great interest for fabricating integrated optical devices [1,2]. Phase holograms formed in strip and planar waveguides can be used e.g. as memory cells, modulators or light amplifiers.

A specific photorefractive nonlinearity in LiNbO₃ optical waveguides is the conversion of light from ordinary to extraordinary polarization. The mechanism of coupling of orthogonally polarized modes is explained by writing holographic gratings due to photovoltaic currents [3]. Light is diffracted from these gratings with polarization conversion, which leads to an energy exchange between the modes. At first, the effect was only observed in strip waveguides [4], while it was unclear whether there exists a corresponding process in planar waveguides. Some years later this interaction was observed in strongly iron-doped planar waveguides [5] too.

In this paper we investigate the influence of different crystal orientations and dimensions of waveguides on the coupling strength of orthogonally polarized modes. Predictions of a simple model are compared with experimental results. Measurements of the linear and circular photovoltaic tensor elements as a function of depth in iron- and copper-doped planar LiNbO₃ waveguides are reported, and the influence of titanium is discussed.

2. Mode coupling equations

The polarization-dependent photovoltaic current density [6], following from a phenomenological theory, is given by

$$j_i = \sum_{j,k} (\beta_{ijk}^s + i\beta_{ijk}^a) E_j^* E_k, \quad (1)$$

where $\beta^{s,a}$ are the real linear (symmetric) and circular (antisymmetric) photovoltaic tensor components and $E_{j,k}$ are the interacting light fields.

Now the interaction of two orthogonally polarized modes in a planar y -cut LiNbO₃ waveguide propagating along the x -axis is considered. In this geometry, the tensor component $\beta_{232} = \beta_{223}$ contributes to the modulated photovoltaic current along the y -axis:

$$j_2 = [(\beta_{232}^s + i\beta_{232}^a) A_{TE}^*(x) U_{TE}(y)^* \times U_{TM}(y) A_{TM}(x) \exp(i\Delta kx) + \text{c.c.}], \quad (2)$$

with A as amplitude and U as normalized component of the electric field (mode) of the ordinarily (TM) and extraordinarily (TE) polarized wave. The longitudinal field component of the TM mode is small compared to the transverse one and can be neglected. The photovoltaic current is modulated in the propagation direction with the period $\Lambda = 2\pi/\Delta k = \lambda_0/(n_o^* - n_e^*)$, determined by the difference of the effective refractive indices $n_{o,e}^*$ of the interacting

modes. Here λ_0 is the vacuum light wavelength. Instead of β it is convenient to use β^l defined as $\beta^l = 2\beta / (c\epsilon_0\sqrt{n_o^*n_e^*})$, where c and ϵ_0 are the vacuum light velocity and dielectric field constant.

Neglecting diffusion effects, the total current density in the crystal consists of drift and photovoltaic contributions. The resulting space charge field E_{sc} follows from the continuity equation in form of a differential equation [7] and has, in the considered planar geometry, components in x - and y -direction. The space charge field $E_{sc,2}$ in y -direction leads to a perturbation of the dielectric tensor or a phase grating via the electrooptic effect:

$$\Delta\epsilon_{23} = -n_o^{*2}n_e^{*2}r_{232}E_{sc,2}, \quad (3)$$

where r_{232} is the electrooptic tensor component. The perturbation of the dielectric tensor has unshifted components according to β_{232}^s and components shifted by $\pi/2$ according to β_{232}^a , relative to the isophase surfaces where Δkx is equal to 2π . As it is well known [8], the shifted components lead to a stationary energy exchange between the orthogonally polarized light waves, while the unshifted parts only influence the relative phases.

The coupling equations for orthogonally polarized modes [5,9] can be written in the form:

$$\frac{dA_{TE}}{dx} = \sqrt{\frac{n_o^*h_{TM}}{n_e^*h_{TE}}} (i\gamma'' + \gamma') |A_{TM}|^2 A_{TE} - (\alpha_{TE}/2)A_{TE}, \quad (4)$$

$$\frac{dA_{TM}}{dx} = \sqrt{\frac{n_e^*h_{TE}}{n_o^*h_{TM}}} (i\gamma'' - \gamma') |A_{TE}|^2 A_{TM} - (\alpha_{TM}/2)A_{TM}, \quad (5)$$

with

$$\gamma' = \frac{\omega\epsilon_0 n_o^{*2} n_e^{*2}}{4\sigma} \eta r_{232} \beta_{232}^s, \quad (6)$$

$$\gamma'' = \frac{\omega\epsilon_0 n_o^{*2} n_e^{*2}}{4\sigma} \eta r_{232} \beta_{232}^a, \quad (7)$$

$$\eta = \frac{1}{\sqrt{h_{TE} n_{TM}}} \int U_{TE}^* U_{sc,2} U_{TM} dy. \quad (8)$$

Here h is the effective thickness of the TE and TM mode, according to the normalization $\int U_i^* U_j dy = h_i \delta_{ij}$, σ is the conductivity, α is the absorption coef-

ficient, and ω is the light frequency. The dimensionless factor η accounts for the spatial overlap of the interacting light fields with the space charge field. The spatial distribution of the space charge field, $U_{sc,2}$, is a solution of the differential equation

$$\left(\frac{d^2}{dy^2} - (\Delta k)^2 \right) U_{sc,2}(y) = \frac{-1}{\sigma A_{sc,2}(x)} \frac{d^2}{dy^2} j_2(x, y) = \frac{d^2}{dy^2} [U_{TE}^*(y) U_{TM}(y)], \quad (9)$$

with the separation of the space charge field

$$E_{sc,2}(x, y) = A_{sc,2}(x) U_{sc,2}(y) = -(\beta_{232}^s + i\beta_{232}^a) / \sigma \times A_{TE}(x) A_{TM}(x) e^{i\Delta kz} U_{sc,2}(y). \quad (10)$$

The real part γ' of the coupling constant determines the energy exchange, and the modulus $|i\gamma'' \pm \gamma'|$ the diffraction efficiency. Because of the nonlinearity of the coupling equations (4, 5) they can only be solved by numerical methods ^{#1}.

3. Influence of geometry

To discuss the dependence of the space charge field on the waveguide properties in a simple model, we consider a thin y -cut crystal of thickness $2d$ (fig. 1).

^{#1} An analytical solution for the diffraction efficiency, as described in ref. [5], is not exact. The amplitude of the diffraction grating depends on the modulation $m = \sqrt{I_{TE} I_{TM}} / (I_{TE} + I_{TM})$ of the interacting modes, and the intensities I in the waveguide depend on the strength of energy exchange. Therefore the real part γ' (which has to be calculated numerically) influences the diffraction efficiency.

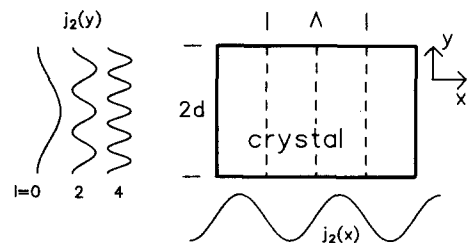


Fig. 1. Thin birefringent y -cut crystal of thickness $2d$. Here $j_2(x)$ is the current density modulation in x -direction, and $j_2(y)$ in y -direction (for various indices l). The dashed lines separate oppositely directed current domains with period $A = \lambda_0 / |n_e - n_o|$.

The photovoltaic current distribution along the y -axis is given by

$$j_2(x, y) = j_0 \cos^2(fy) \exp(i\Delta kx), \quad (11)$$

where j_0 is the current amplitude, $\Delta k = 2\pi/\Lambda$, and $f = (l+1)\pi/2d$ with $l=0, 2, 4, \dots$. Instead of the complicated results in ref. [7], this model enables a simple solution of eq. (9). With the boundary conditions $E_{sc,2}(y = \pm d) = 0$ one obtains

$$E_{sc,2}(x, y) = \frac{2j_0 f^2}{\sigma[4f^2 + (\Delta k)^2]} \left(1 - 2 \cos^2(fy) - \frac{\cosh(\Delta ky)}{\cosh(\Delta kd)} \right) \exp(i\Delta kz). \quad (12)$$

It should be noticed that the maximum of the field is always smaller than j_0/σ .

The amplitude of the space charge field depends on the ratio of grating period Λ and crystal thickness $2d$. With decreasing thickness $2d$, the amplitude increases and reaches constant values for $\Lambda/2d \gg 1$. In the case of thick crystals, $\Lambda/2d \ll 1$, the space charge field vanishes. This is the reason why no coupling of colinearly propagating, orthogonally polarized waves in bulk crystals is observed [10], when the beam size is much larger than the grating period Λ . Only if the two copropagating waves form an angle different from zero, they may be coupled.

In y - and z -cut strip waveguides, and also in y -cut planar waveguides, the effective thickness of the waveguiding structure in the direction of the photovoltaic current is comparable to the grating period, which is typically 5–10 μm in LiNbO_3 . This leads to a nonvanishing space charge field, and therefore to coupling of orthogonally polarized modes. In planar z -cut waveguides, the amplitude of the space charge field depends on the ratio of grating period Λ and beam size (aperture) of the excited mode. Usually, the beam size is much larger than the grating period, thus no or only small mode coupling is expected.

In the case of counterpropagating orthogonally polarized modes, the grating period Λ is of the order of some tens of nanometers ($\Lambda = \lambda_0 / (n_o^* + n_e^*)$). Now Λ is small compared to the thickness of the waveguiding structures, and the space charge field vanishes in strip waveguides and y -cut planar waveguides, too.

Figure 2 shows the spatial dependence of the space

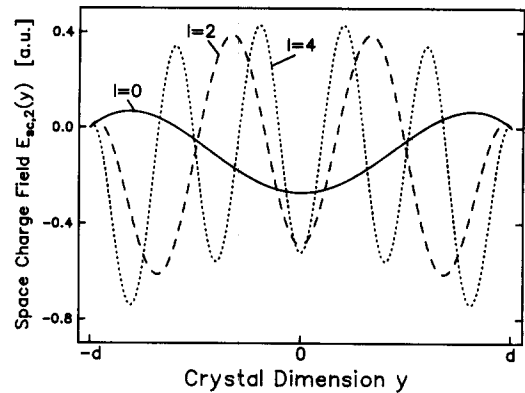


Fig. 2. Spatial distribution of the space charge field $E_{sc,2}(y)$ for $\Lambda = 2d$ and different current modulation frequencies $f = (l+1)\pi/2d$ (here $l=0, 2$ and 4).

charge field for current distributions with different index l . Here the quotient $\Lambda/2d = 1$ and the amplitude j_0 are kept constant. With increasing index l , there is a higher modulation frequency of the current along the y -axis. Because of the second derivative in eq. (9), this leads to an increased space charge field. If the effective thicknesses of coupled modes are similar, one expects stronger coupling for modes with higher index.

For refractive index profiles of metal-indiffused waveguides (nearly gaussian refractive index profiles), the situation is more complicated. The electric fields of the waveguide modes have to be reconstructed by numerical methods, and no analytical solution of eq. (9) is possible. The photovoltaic tensor elements β are proportional to the concentration of photorefractive filled traps, e.g. Fe^{2+} or Cu^+ , and often these concentrations are not homogeneous over the waveguide depth. In non-step refractive index profiles, the effective thickness of the excited modes increases with increasing mode index. This leads to a reduced space charge field. On the other hand, the higher current modulation frequency for higher modes gives a higher amplitude of the space charge field. One can expect a partial compensation of the two effects described above, when considering the dependence of the space charged field on mode index.

In summary we conclude that there is no or only small mode interaction for counterpropagating light waves. The same is true for colinearly propagating waves in z -cut waveguides. In y -cut waveguides,

however, we expect coupling effects for colinearly propagating waves, but no significant dependence of the coupling strength on mode index.

4. Experimental arrangement

Our waveguides are prepared by titanium-indiffusion (60–160 nm Ti films, annealed 20–80 h at 1000 °C) in nominally pure y - and z -cut lithium niobate crystals. To reach higher photorefractive sensitivity, iron films (50–80 nm) are indiffused additionally in the same manner as titanium. For comparison, waveguides with copper doping are fabricated, too. The content of iron and copper, respectively, at the surface of the waveguiding layer is measured by X-ray photoelectron spectroscopy (XPS) to be of the order of several promille. Due to these large concentrations the waveguides exhibit high dark conductivity which considerably exceeds photoconductivity.

The experimental setup is shown in fig. 3. Light of the green line (514.5 nm) of an Ar⁺ ion laser is coupled into two polarization conserving monomode fibers. Two computer controlled rotary states allow the excitation of TE and TM modes independent of each other. Rutil prisms are used to couple radiation into and out of the waveguide with an efficiency of nearly seventy percent.

5. Results and discussion

At first we consider holographic scattering effects, which provide information on coupling direction and

spatial dependence of coupling constants; of special interest are the values for copropagating waves. When exciting ordinarily polarized modes in y - and z -cut waveguides, light scattered into extraordinarily polarized modes is amplified. The spatial distribution of the amplified light is different for the two cuts.

For y -cut waveguides, the maximum of TE-polarized light is in the direction of the excited TM mode (fig. 4), indicating strong coupling of copropagating waves. In z -cut waveguides, we observe two maxima of TM-polarized amplified light at symmetric angles θ (measured in the waveguiding layer relative to the propagation direction of the incoupled TE light), while in propagation direction the intensity of the amplified scattered light and therefore coupling is small (fig. 4). The distributions are determined by the initial straylight, which is strongest in the propagation direction of the excited mode, and by an angle dependent amplification factor. The results for z -cut waveguides are analogous to those of wide angles anisotropic scattering in volume crystals [11], where the amplification factor is zero for copropagating waves and increases with growing scattering angle to a broad maximum at $\theta \approx 15^\circ$ [12]. For these large scattering angles, however, the initial straylight is small. Furthermore, the measured distribution of amplified light is limited because of the small area between prism and waveguide which allows tunneling of light (a typical diameter of this area is 1 mm). This explains qualitatively the position of the maxima at the angles $\theta \approx \pm 2.5^\circ$.

The results of holographic scattering are consistent with those of mode coupling experiments, where both, ordinarily and extraordinarily polarized modes, are excited externally. We do not observe any cou-

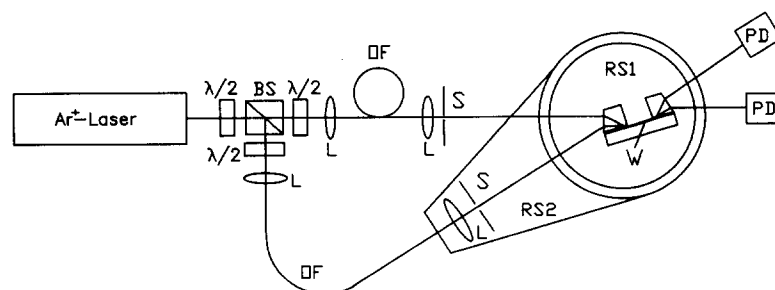


Fig. 3. Experimental arrangement for coupling measurements of orthogonally polarized waveguide modes. BS: polarizing beamsplitter, $\lambda/2$: $\lambda/2$ -plate, L: microscope lens, OF: optical fiber, S: shutter, RS: rotary stage and PD: photodetector.

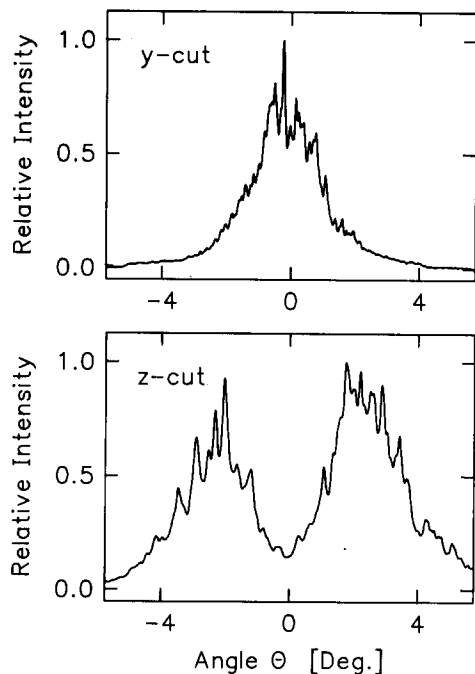


Fig. 4. Spatial distribution of the extraordinary straylight in y -cut and z -cut waveguides for excitation with ordinary light. The angle θ is measured in the waveguide layer relative to the propagation direction of the excited beam.

pling of colinearly propagating modes with orthogonal polarization in z -cut waveguides for beam diameters up to 0.3 mm. In y -cut waveguides, however, strong coupling with nearly full energy transfer for a few millimeters of propagation length is obtained. Furthermore, no energy exchange between orthogonally polarized counterpropagating beams in y - and z -cut waveguides is measured.

Figure 5 shows the coupling and diffraction characteristics of the interaction of the TE_5 and TM_5 mode copropagating in an iron-doped y -cut waveguide. We observe similar effects for other modes, as the overlap factor η is nearly the same for all mode combinations. At the moment the two beams are switched on ($t=0$), energy is transferred from the TM to the TE mode. After sufficient time the out-coupled power of the two modes reaches stationary values, and at $t=60$ s one of the beams is switched off. Light is now diffracted, and the written grating decays. While the power of the light transferred from the TE to the TM mode decreases to zero, there remains always some power in the TE mode when the

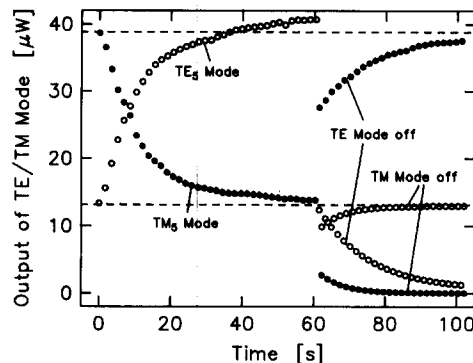


Fig. 5. Output power of TE (\circ) and TM mode (\bullet) in a typical coupling measurement. Up to $t=60$ s power is transferred from the TM mode to the TE mode. At $t=60$ s one mode is switched off, and power is diffracted to the orthogonally polarized mode. The dashed lines represent the power in the two modes without energy exchange.

TM mode is diffracted. This is due to coupling of the excited TM mode and TE-polarized straylight, where the straylight is amplified.

When reading the diffraction grating continuously, the decay of the grating is caused by charge redistribution due to dark- and photoconductivity. If TE-polarized read-out light is used, this TE mode and the TM mode, generated by diffraction, write a new grating which is shifted by π with respect to the already recorded grating [13]. For this reason we observe enhanced erasure. If we use TM-polarized light for read-out, the TM mode and the generated TE mode write a grating which is in phase with the existing one. In this case we observe an increased erasure time.

By inserting the experimental data ($A(x=0)$, n^* , h , α , coupling length $x=x_0$, σ and η) into eqs. (4), (5) and fitting γ' to the measured values of energy exchange, we obtain results for the photovoltaic tensor element $\beta_{232}^{\alpha I}$. Here the imaginary part γ'' of the coupling constant has no influence.

Now the diffraction grating is assumed to be stationary. To obtain $|i\gamma'' \pm \gamma'|$, the x -dependent terms $A_{TE}^* A_{TM}$ and $A_{TM}^* A_{TE}$ in eqs. (4), (5) are kept constant. The start values of these terms are taken from the last fit of γ' . Then the imaginary part γ'' is varied, and the equations are now fitted to the measured values of diffraction efficiency, with either $A_{TE}(x=0)$ or $A_{TM}(x=0)$ equal to zero. Then γ'' is inserted again

in eqs. (4), (5) to obtain new values for the functions $A_{TE}^* A_{TM}$ and $A_{TM}^* A_{TE}$. After iteration a self-consistent solution is found yielding $|i\gamma'' \pm \gamma'|$. From the relation $|\beta_{232}^{a,l}| \propto |\gamma''|$ and with the known value of γ' we finally determine $|\beta_{232}^{a,l}|$.

In fig. 6 the results for a γ -cut waveguide are shown as a function of effective depth. The effective depth is given by the center of the overlap integral η . The values of $\beta_{232}^{a,l}$ are of the same order of magnitude as those of heavily doped bulk crystals [12]. However, while in iron-doped bulk crystals the symmetric tensor component is one order lower than the antisymmetric one, in our waveguides $|\beta_{232}^{a,l}|$ is only slightly smaller than the absolute value of $\beta_{232}^{a,l}$.

The values for both $|\beta_{232}^{a,l}|$ and $\beta_{232}^{a,l}$ are reduced for lower modes propagating near the surface of the waveguiding layer. Because the concentration of Fe^{2+} is highest at the surface, one should expect the largest values of photovoltaic tensor elements for the lowest modes. For this reason we deduce from the experimental results that the photovoltaic tensor elements $\beta_{232}^{a,l}$ are diminished due to the influence of the high titanium concentration at the surface.

In the investigated copper-doped waveguides, the direction of coupling between TE- and TM-polarized light is the same as for iron doping, i.e. the extraordinarily polarized light is amplified. For this reason the sign of the tensor component $\beta_{232}^{a,l}$ is op-

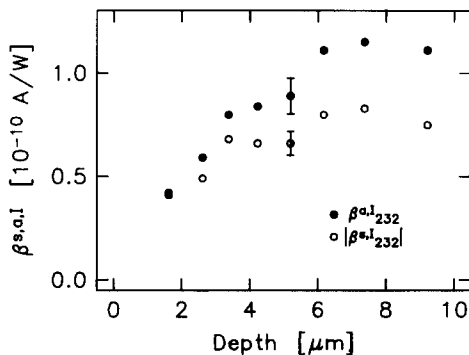


Fig. 6. Experimental values of linear ($|\beta_{232}^{a,l}|$) and circular ($\beta_{232}^{a,l}$) photovoltaic constants as a function of waveguide depth measured with different mode combinations. This waveguide is fabricated by vacuum deposition of 160 nm Ti, annealing 52 h at 1000 °C in wet argon gas, then deposition of 60 nm Fe, and annealing additionally 32 h in wet oxygen.

posite to that of bulk crystals [14]. This is another evidence for the influence of titanium on the non-diagonal elements of the photovoltaic tensor.

In summary we have shown that the conclusions derived from our model concerning the influence of the geometric waveguide properties on polarisation conversion, can be verified very well experimentally. Furthermore, the described method for the determination of the non-diagonal elements of the photovoltaic tensor elucidates differences of the material properties of bulk crystals and doped waveguides, e.g. the influence of titanium on the photovoltaic constants.

Acknowledgements

We thank T. Albers and M. Neumann for the XPS measurements. Financial support of the Deutsche Forschungsgemeinschaft (SFB 225, D9) is gratefully acknowledged.

References

- [1] V.E. Wood, P.J. Cressman, R.L. Holman and C.M. Verber, in: Photorefractive materials and their applications, Vol. 62 of Topics of applied physics (Springer, Berlin, 1989).
- [2] A. Donaldson, J. Phys. D 24 (1991) 785.
- [3] S.I. Bozhevolyai, E.M. Zolotov, P.G. Kazanskii, A.M. Prokhorov and V.A. Chernykh, Sov. Techn. Phys. Lett. 9 (1983) 297.
- [4] E.M. Zolotov, P.G. Kazanskii and V.A. Chernykh, Sov. Techn. Phys. Lett. 7 (1981) 397.
- [5] I.I. Itkin and S.M. Shandarov, Sov. Tech. Phys. Lett. 16 (1990) 357.
- [6] V.I. Belinicher and B.I. Sturman, Sov. Phys.-Uspheki 23 (1980) 199.
- [7] I.I. Itkin and S.M. Shandarov, Sov. Avtometriya 4 (1989) 72.
- [8] N.V. Kukhtarev, V.B. Markov, S.G. Odoulov, M.S. Soskin and V.L. Vinetskii, Ferroelectrics 22 (1979) 946.
- [9] J.F. Lam and H.W. Yen, Appl. Phys. Lett. 45 (1984) 1172.
- [10] S.G. Odoulov, Ferroelectrics 91 (1989) 213.
- [11] E. Avakyan, S. Allaverdyan, K. Belabaev, V. Sarkisov and K. Toumanyanyan, Sov. Solid State Phys. 20 (1978) 1401.
- [12] A. Novikov, S. Odoulov, O. Oleinik and B. Sturman, Ferroelectrics 75 (1987) 295.
- [13] D.L. Staebler and J.J. Amodei, J. Appl. Phys. 43 (1972) 1042.
- [14] I.N. Kiseleva, V.V. Obukhovskii and S.G. Odoulov, Sov. Phys. Solid State 28 (1986) 1673.